Macromolecules

Article

Confined Crystallization and Morphology of Melt Segregated PLLA-*b*-PE and PLDA-*b*-PE Diblock Copolymers

Reina Vero#nica Castillo, Alejandro J. Mu#ller, Ming-Champ Lin, Hsin-Lung Chen, U-Ser Jeng, and Marc A. Hillmyer

Macromolecules, **2008**, 41 (16), 6154-6164 • DOI: 10.1021/ma800859y • Publication Date (Web): 15 July 2008

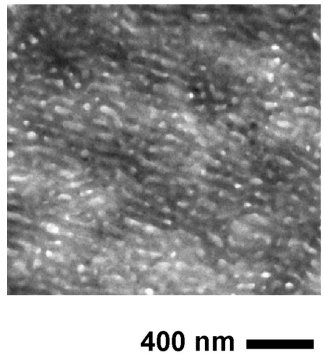

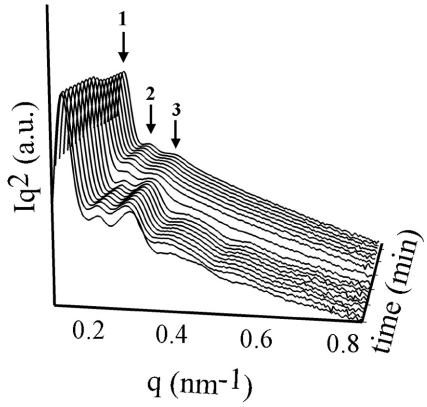

More About This Article

Additional resources and features associated with this article are available within the HTML version:

- Supporting Information
- Access to high resolution figures
- Links to articles and content related to this article
- Copyright permission to reproduce figures and/or text from this article

View the Full Text HTML

Confined Crystallization and Morphology of Melt Segregated PLLA-*b*-PE and PLDA-*b*-PE Diblock Copolymers

Reina Verónica Castillo,[†] Alejandro J. Müller,*[,†] Ming-Champ Lin,[‡] Hsin-Lung Chen,*[,‡] U-Ser Jeng,[§] and Marc A. Hillmyer[||]

Departamento de Ciencia de los Materiales, Grupo de Polímeros USB, Apartado 89000-A, Caracas, Venezuela; Department of Chemical Engineering, National Tsing Hua University, Hsin-Chu 30013, Taiwan; National Synchrotron Radiation Research Center, Hsin-Chu 300, Taiwan; and Department of Chemistry, University of Minnesota, 207 Pleasant Street SE, Minneapolis, Minnesota 55455-0431

Received April 17, 2008; Revised Manuscript Received June 10, 2008

ABSTRACT: The crystallization behavior of strongly segregated diblock copolymers composed of polyethylene (PE) and poly(L-lactide) or racemic poly(lactide) (PLA) blocks has been investigated by differential scanning calorimetry (DSC), small-angle X-ray scattering (SAXS), wide-angle X-ray scattering (WAXS), and transmission electron microscopy (TEM). In both systems the crystallization of PE block was confined within the preexisting lamellar domain. In the double-crystalline PLLA-*b*-PE, coincident crystallization of PLLA and PE blocks was observed during cooling process because the crystallization rate of the PLLA block was retarded by the covalent linkage with the PE block. When the PLLA block was self-nucleated, a complete separation of the crystallization process of both blocks was achieved. Polarized optical microscopy confirmed that neither PLLA nor PE blocks could form spherulites in view of the large segregation strength that effectively confined the crystallization within the lamellar microdomains. High-speed DSC was applied to reduce reorganization during the scan so that values closer to the equilibrium melting points ($T_m°$), employing the Hoffman−Weeks treatment, could be obtained for PLLA. The $T_m°$ for the PLLA block was depressed as compared to homo-PLLA by confinement effects. The crystallization of the PE block within the amorphous−crystalline PLDA-*b*-PE was strictly confined, and the microdomain morphology established in the melt state was essentially unperturbed, regardless of whether the crystallization occurred when the PLDA block was glassy or rubbery (hard or soft confinement). In the case of the double-crystalline PLLA-*b*-PE system, the crystallizations of both PE and PLLA blocks were also effectively confined within the respective lamellar microdomains, irrespective of which is the leading crystallizing component prescribed by the crystallization history. The confinement effect was a consequence of the large segregation strength coupled with the solidification of the microdomains of the leading crystallizing component, which subsequently imposed a hard confinement effect on the crystallization of the second block. TEM revealed the ordered lamellar morphology, and in one case the crystalline lamellae of the PE block were visualized within the microphase-separated lamellae due to an isothermal crystallization pretreatment.

Introduction

Crystallization and spatially ordered structure formation in block copolymers with crystallizable blocks have attracted significant attention in the past decade.[1−22] The various morphologies are generated depending on the segregation strength and the relative values of the order−disorder transition temperature (T_{ODT}), the crystallization temperature (T_c), and the glass transition temperature (T_g). When the crystallization is produced after quenching from the disordered melt state, the final solid-state structure is determined by a complex interplay between microphase separation and crystallization.[4,5] However, when crystallization occurs from microphase-separated melt, the final morphology will strongly depend on the relative location of the crystallization temperature and the glass transition temperature for amorphous−crystalline block copolymers. As $T_{ODT} > T_c > T_g$, the crystallization can provoke a breakout from the ordered melt and formed a new morphology.[4,8,9,23,24] Of course, whether crystallization destroys the microphase separation structure or not is also related to the segregation strength. As $T_{ODT} > T_g > T_c$, for a block copolymer having a glassy amorphous component, the crystallization will be confined within the microdomain structure determined by phase segregation.[24−31]

Most research so far has focused on block copolymers where only one of the blocks can crystallize.[1−3] The crystallization behavior of block copolymers containing two crystalline components has been recently reported;[32−48] however, double-crystalline diblock copolymers have not been investigated so extensively because of the complexity associated with the competitive crystallization of the two blocks. When the crystallization in such double-crystalline diblock copolymers is considered, the competition among the crystalline components and the interplay between crystallization and microphase separation will be very important. Generally speaking, if crystallization of the leading component (the one crystallizing at higher temperatures) should destroy the microphase separation established in the melt, the other component crystallizes within the spatial environment prescribed by the crystalline lamellae of the leading component. Consequently, the behavior of the component that crystallizes first upon cooling from the melt becomes an important factor that determines the final structure and the relationship between the melting temperature values of these two crystalline components could be very significant as nucleation and confinement effects can arise [ref 3 and references therein]. On the other hand, if the overall melt structure is retained in strongly segregated systems, crystallization occurs within the nanoscale domains, and phenomena like fractionated crystallization and first-order crystallization kinetics could arise depending on composition.[2,3,5,8,18,24,46]

According to the previous studies on double-crystalline systems where the crystallization process destroys the possible

* Corresponding authors.
[†] Grupo de Polímeros USB.
[‡] National Tsing Hua University.
[§] National Synchrotron Radiation Research Center.
[||] University of Minnesota.

10.1021/ma800859y CCC: $40.75
Published on Web 07/15/2008

melt morphology, if separated crystallization of two blocks occurs, the higher T_m block crystallizes first to form a lamellar morphology followed by the crystallization of the lower T_m block starting from this lamellar morphology. Hamley et al. reported poly(ϵ-caprolactone) crystallized within poly(L-lactide) crystal lamellae which was previously forming spherulites after quenching from the miscible melt state in PLLA-*b*-PCL diblock copolymer.[44,45] Nojima et al. explored the crystallization and melt-quenched morphology of poly(ϵ-caprolactone)-*block*-poly(ethylene).[47] Albuerne et al. investigated the crystallization of poly(*p*-dioxanone)-*block*-poly(ϵ-caprolactone). They found that the two blocks crystallized in a single coincident exotherm upon cooling from the melt. On the other hand, the crystallized PPDX acts as nucleating agent for PCL so that the crystallization kinetics of the PCL in the copolymers is accelerated.[42] Hillmyer and Bates explored poly(ethylene)−poly(ethylene oxide) diblock copolymers and showed that poly(ethylene) crystallization can lead to disruption of the melt ordered phase.[49] Sun et al. also employed poly(ethylene)-*block*-poly(ethylene oxide). They investigated the crystal orientation and calculated the interlamellar distance in different crystallization temperature region.[48]

Takeshita et al. focused on the formation of crystal lamellar structure in poly(ethylene glycol)-*block*-poly(ϵ-caprolactone) having two crystalline blocks whose melting temperatures are within 10 °C. They concluded that PCL crystallized first followed by the crystallization of PEG with preservation of the PCL crystal lamellar morphology. This means that PEG must crystallize within the confined space between the formerly formed PCL crystal lamellae in a similar way to the already cited works on PPDX-*b*-PCL and PLLA-*b*-PCL.[3,42–46,50] Ring et al.[51] recently reported the synthesis of PE-*b*-PLLA block copolymers with 12−29 kg/mol and 89−96 wt % of PLLA, combining catalytic ethylene oligomerization with "coordinate-insertion" ring-opening polymerization. They reported microphase separation observed by AFM although spherulites were detected by POM during isothermal crystallization after erasing thermal history at 200 °C for 3 min. The effect of thermal degradation was not considered.

In this work, the amorphous−crystalline poly(LD-lactide)-*b*-poly(ethylene) and double-crystalline poly(L-lactide)-*b*-poly(ethylene) systems were investigated. Polylactide is a biodegradable aliphatic polyester derived from renewable resources and has gained much interest in recent years. There are three commonly types of polylactide: poly(L-lactide) (PLLA), poly(D-lactide) (PDLA), and poly(LD-lactide) (PLDA). Poly(L-lactide) and poly(D-lactide) are both semicrystalline materials as a result of stereoregularity. However, poly(LD-lactide) is a racemic amorphous material formed by the copolymerization of L-lactide and D-lactide. Currently, polylactide is used for biomedical applications[52] such as sutures and drug delivery devices because of its biodegradable and biocompatible nature, but its use has now extended to biodegradable packaging applications as well as bottles.

The amorphous−crystalline poly(LD-lactide)-*b*-poly(ethylene) and double-crystalline poly(L-lactide)-*b*-poly(ethylene) are strongly segregated; in fact, a rough estimation based on the molecular weight of the blocks employed in this work and their solubility parameters yields values of the segregation strength parameter (i.e., χN^1) larger than 350. Thus, for composition close to 50 wt % melt-segregated lamellar microdomains are expected.[53,54] Previous works[53,54] revealed that the overall isothermal crystallization rate of the PLLA block was slowed down as compared to homo-PLLA by the covalently bonded PE chains that were in the melt at the PLLA crystallization temperatures. This depression of the crystallization rate of the PLLA block within the copolymer produces a coincident crystallization process (where both PE and PLLA crystallize) when PLLA-*b*-PE is cooled down from the melt at cooling rates larger than 2 °C/min.[53] A nucleation effect of PLLA on the PE block was detected, whereby the overall crystallization rate of the PE block is faster when it is covalently bonded to previously crystallized PLLA than when it is bonded to a rubbery PLDA block; however, higher supercooling values are needed in order to crystallize the PE chains within both block copolymers as compared to the respective homopolymer.[54] The Avrami indexes obtained by fitting DSC isothermal crystallization data revealed higher values for the PLLA block as compared to homo-PLLA; this was rationalized as a sign of nucleation restrictions on the PLLA block which renders nucleation more sporadic.[53] On the other hand, the PE block within the block copolymers exhibits lower Avrami index values than those observed for homo-PE. This decrease was due to dimensionality restrictions imposed by the lamellar microdomain morphology confinement. As a matter of fact, no spherulites were observed for these diblock copolymers with lamellar microdomain morphologies, as expected for strongly segregated diblock copolymers.[2,3] Therefore, two-dimensional lamellar crystallization arrangements within the microphase-separated domains were the predominant morphology for the PE block.[53]

Table 1. Molecular Characteristics of the Block Copolymers and Homopolymers

copolymers	PLA/PE exp composition[a]	$\bar{M}_n$ (kg mol^{-1})[b] PLA block	$\bar{M}_n$ (kg mol^{-1})[b] PE block	PE % 1,2 units	I[c]
$PLLA^{24}$	100/0	24.1			1.16
$L_{46}E_{54}^{50}$	46/54	22.5	26.5	7.2	
$LD_{54}E_{46}^{60}$	54/46	32.4	27.7	7.0	
PE^{28}	0/100		28.0	7.0	

[a] Experimental compositions as determined by ^{1}H NMR spectroscopy. [b] Experimental $\bar{M}_n$ estimated by ^{1}H NMR spectroscopy. [c] Polydispersity index determined by SEC.

In this work, amorphous−crystalline poly(LD-lactide)-*b*-poly(ethylene) and double-crystalline poly(L-lactide)-*b*-poly(ethylene) diblock copolymers were evaluated by self-nucleation studies to explore the confinement effect caused by one block on the other as compared to the free crystallization experienced by the respective homopolymers. Also, the equilibrium melting point of the PLLA block as compared to homo-PLLA was determined by the Hoffman−Weeks approach after isothermal crystallization. In addition, the morphology was studied by simultaneous small-angle and wide-angle X-ray scattering (SAXS/WAXS) and by transmission electron microscopy (TEM); different thermal treatments were employed to investigate the degree of possible distortion of the microdomain morphology after the crystallization of one or two blocks.

Experimental Section

Materials. The samples used in this study were amorphous−crystalline PLDA-*b*-PE and double-crystalline PLLA-*b*-PE diblock copolymers. The synthetic procedure of PLDA-*b*-PE and PLLA-*b*-PE was already published in previous literature.[55,56] Briefly, 1,3-butadiene was anionically polymerized in cyclohexane using *sec*-butyllithium as the initiator and subsequently end-capped with ethylene oxide to give hydroxyl-terminated 1,4-polybutadiene containing ca. 93% of the 1,4-regioisomer. This polybutadiene was then hydrogenated to give hydroxyl-terminated polyethylene, which was utilized in combination with $AlEt_3$ as a macroinitiator in the ring-opening polymerization of L-lactide (PLLA) or LD-lactide (PLDA). The molecular characterization was determined by size exclusion chromatography (SEC) and ^{1}H NMR spectroscopy as shown in Table 1. The diblock copolymer that we have used in Table 1 denotes the PLLA block as L, PLDA block as LD, and the PE block as E; the subscripts indicate the composition in wt %, and superscripts indicate the approximate number-average molecular weight in kg/mol.

Differential Scanning Calorimetry (DSC). DSC experiments were carried out on a Perkin-Elmer DSC-7 instrument to study the

Table 2. Thermal Properties Obtained from DSC Scans

	PLA					PE			
sample	T_c, °C	T_m, °C	ΔH_c, J g^{-1}	ΔH_m, J g^{-1}	T_g, °C	T_c, °C	T_m, °C	ΔH_c, J g^{-1}	ΔH_m, J g^{-1}
PLLA[24]	107.5	173.9	31	40	63.2[a]				
$L_{46}E_{54}$[50]		171.7		39	62.1	88.7	104.2	*b*	*b*
$LD_{54}E_{46}$[60]					55.0	88.3	103.5	109	115
PE[28]						94.3	107.5	105	110

[a] Measured after quenching the simple to room temperature. [b] Signals are overlapped during cooling by coincident crystallization and during heating by PLLA cold crystallization.

isothermal crystallization and melting behaviors of the diblock copolymers. Samples were encapsulated in aluminum pans, and their mass was ~5 mg. The calibration was performed with indium and hexatricontane, and all tests were run employing ultrapure nitrogen as purge gas.

In the standard DSC experiments, the samples were first heated to a temperature of ~20 °C higher than the melting point of either PLLA or PE blocks and kept at that temperature for 3 min in order to erase thermal history. Then a cooling run at 10 °C/min was recorded down to −20 °C, followed by a subsequent heating run performed also at 10 °C/min.

In the isothermal crystallization experiments, for the PLLA block within PLLA-*b*-PE, the pretreatment was performed in the same way as in the standard DSC experiments. After erasing thermal history, the samples were immediately cooled (at 60 °C/min) to the isothermal crystallization temperature, and then the crystallization process was recorded as a function of time.

High-speed DSC was performed in a Perkin-Elmer Pyris 1. Heating scans at 80 and 100 °C/min after isothermal crystallization were employed to minimize reorganization phenomena during heating, as was reported by Pijpers et al.[57] To avoid as much as possible thermal lag (superheating effects), the sample mass was reduced (from 5 to 0.63−0.5 mg) in the same factor that the scan rate was increased (from 10 to 80−100 °C/min, respectively).[57] The experiments were performed in a DSC without any modification, so the linearity of the temperature−time relationship during the measurement (during heating) was confirmed.

Small-Angle X-ray Scattering (SAXS) and Wide-Angle X-ray Scattering (WAXS). Simultaneous small-angle and wide-angle X-ray scattering experiments were performed at station 17B3 at the National Synchrotron Radiation Research Center (NSRRC) located at Hsin-Chu, Taiwan. The time necessary for each data collection was 5 min. The SAXS intensities obtained were plotted against $q = 4\pi \sin \theta/\lambda$, where λ is the wavelength of X-ray (λ = 0.155 nm) and 2θ is the scattering angle. The beam center was calibrated using silver behenate with the primary reflection peak at 1.067 nm^{-1}. We focused our attention on the angular positions of scattering peaks arising from the lamellar morphology because they were intimately related to the morphology formed in the system and also straightforwardly obtained from the SAXS curves. The WAXS diffraction patterns covering the scattering vector range q = 10−22 nm^{-1} were recorded simultaneously with the SAXS profiles. The WAXS angular scale was calibrated using silicon, sodalite, and high-density polyethylene.

Transmission Electron Microscopy. The bulk morphology of the PLLA-*b*-PE and PLDA-*b*-PE diblock copolymers was examined in a JEOL 1220 TEM operated at 100 kV. Small pieces of the diblock copolymers were first stained by immersion in 1% RuO_4 stabilized aqueous solution during 24 h. After staining, the small pieces were sectioned in a LEICA M3Z ultramicrotome at room temperature. Ultrathin sections of ~50 μm were obtained using a diamond knife and were stained again with vapors of the 1% RuO_4 stabilized aqueous solution.

Results and Discussion

Standard DSC Results. Standard DSC cooling and subsequent heating scans at 10 °C/min for homo-PLLA, PLLA-*b*-PE, PLDA-*b*-PE, and homo-PE were previously reported,[53,54] and all relevant thermal properties extracted from these results are presented in Table 2. The PLLA-*b*-PE diblock copolymer exhibits as expected two well-defined fusion endotherms, while both blocks crystallized unexpectedly in a single coincident exotherm upon cooling from the melt (reported as T_c of polyethylene in Table 2).

The coincident crystallization process is a consequence of the restrictions supplied to the crystallization of the PLLA block by the molten PE block. That means the crystallization kinetics of PLLA block is strongly retarded during the cooling process from the melt at 10 °C/min (as compared to homo-PLLA crystallization), and its delayed crystallization process overlaps with that of the PE block which starts to crystallize at lower temperatures. This coincident crystallization was confirmed in a previous study.[53] It was determined that some fraction of the PLLA block crystallizes in a coincident fashion with the PE block whenever the cooling from the melt is performed at rates higher than 2 °C/min. During the subsequent heating, most of the PLLA crystallizes, and this cold crystallization overlaps with the melting of the PE block and produces an apparently bimodal fusion; details can be found in ref 53. Similar delayed crystallization kinetics as compared to parent homopolymers have already been reported for PPDX-*b*-PCL (poly(*p*-dioxanone)-*block*-poly(ϵ-caprolactone), PE-*b*-aPP (polyethylene-*block*-atactic polypropylene), and PEO-*b*-PB (poly(ethylene oxide)-*block*-polybutadiene).[16,43,58] Furthermore, the crystallization process of both blocks can be separated by employing a slower cooling rate, as was previously reported,[53] or by self-nucleating the PLLA block as will be shown below.

The T_g of both the PLLA block and the PLDA blocks are reported in Table 2. Table 2 also reports the T_g value for homo-PLLA obtained by quenching the sample in order to prevent its crystallization and then heating it in the DSC. The value obtained (63.2 °C) is very similar to that of the PLLA block within the PLLA-*b*-PE diblock copolymer, as expected for a strongly segregated copolymer. The T_g of the PLDA block can be clearly identified at 55 °C. The value of the T_g is lower than that corresponding to PLLA in view of its different stereoregularity, which prevents its crystallization process. There are literature reports that indicate a shift in the glass transition of PLLA as crystallinity increases, since the segmental relaxation is altered by the presence of a crystalline phase.[59,60]

The PE block within the $L_{46}E_{54}$[50] crystallizes in a coincident fashion with PLLA block at a peak temperature of 88.7 °C, while the PE block within $LD_{54}E_{46}$[60]crystallizes with a peak at 88.3 °C. If the PLLA block is crystallized until saturation at temperatures where the PE block is molten (130 °C) and then later cooled down, a stronger nucleation effect of the PLLA on the PE can be observed.[53] This fact will be reflected further below on the self-nucleation of the PLLA block and was also reflected in the crystallization kinetics of the PE block previously reported.[53,54] However, in spite of the nucleation effect, the PE block within both block copolymers crystallizes at lower temperatures than the homo-PE (94.3 °C) due to topological restrictions. The melting temperature of both blocks decreased within the diblock copolymers with respect to the parent homopolymers, a reflection of their lower crystallization temperatures which probably produce thinner lamellae.

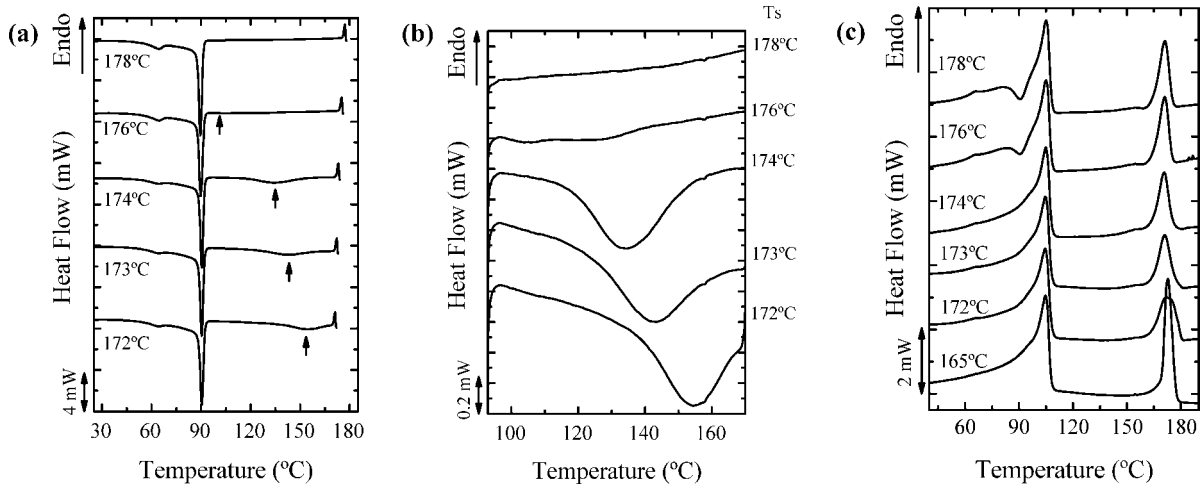

Figure 1. (a) DSC cooling scans at 10 °C/min after self-nucleation of the $L_{46}E_{54}^{50}$ block copolymer at the indicated self-nucleation temperatures (T_s). (b) A close-up of (a). (c) Subsequent heating scans at 10 °C/min.

Self-Nucleation Studies for the PLLA Block. The self-nucleation technique was employed in order to study in detail the effect of self-nuclei on the crystallization behavior of both crystallizable blocks and homopolymers. Details of the experimental method can be found in previous works.[61–63] Briefly, the samples are first heated to a temperature high enough to completely melt the polymer in order to erase crystalline thermal history; then they are cooled at 10 °C/min down to −20 °C to provide them with a standard thermal history. During this standard cooling the polymer will crystallize by heterogeneous nucleation on existing temperature-resistant heterogeneities. Then the samples are heated once more but this time up to a temperature denoted T_s (or self-nucleation temperature) and isothermally kept there for 3 min. After treatment at T_s, the sample is cooled down to −20 °C (examples of such cooling scans can be seen in Figure 1) and subsequently heated at 10 °C/min until full melting occurs. Depending on T_s, the sample can be in one of three general domains: In domain I the sample is completely molten; in domain II the sample is self-nucleated since T_s is high enough to melt almost all crystals but low enough to produce self-seeds (which may arise from crystal fragments or crystallization precursors, see ref 63 for further details), and therefore the nucleation density can be enormously increased; in domain III, the sample is partially molten so that self-nucleation and annealing of unmelted crystals will take place at T_s.

Figure 1 shows DSC cooling scans after 3 min at the indicated T_s temperatures for $L_{46}E_{54}^{50}$. During the whole self-nucleation process of the PLLA block in this copolymer, the PE block remains molten because of the temperatures involved. At T_s = 178 °C a single crystallization exotherm (in Figure 1a) is observed due to the coincident crystallization previously explained, and the subsequent heating scan (Figure 1c) shows the two well-defined endotherms with the apparently bimodal fusion of the PE block. If T_s temperatures equal to or higher than 178 °C are employed, the PLLA crystallizes always at the same temperature (and coincidentally with the PE block). Therefore, the sample at 178 °C is in domain I, i.e., the complete melting domain.

When a T_s of 176 °C is employed, the PLLA block is now self-nucleated, and a new high-temperature exotherm emerges just before the PE block starts to crystallize. At T_s = 176 °C, the PLLA is in domain II and lowering T_s leads to a clear separation of the crystallization exotherms of the PLLA and the PE block during cooling after self-nucleation; this is shown in Figure 1a and in the close-up of the high-temperature region presented in Figure 1b. The increase in nucleation density provided by self-nucleation causes a shift in crystallization temperature of the PLLA block but also an increase in the enthalpy of crystallization that can be attained during cooling from the melt. The enthalpies of crystallization of the PLLA block for T_s temperatures of 174−172 °C (see Figure 1b) are still lower than the corresponding melting enthalpies upon subsequent heating (Figure 1c), although the difference is not large. Two possibilities may explain this discrepancy. The self-nucleation procedure may not have been 100% effective or reorganization effects during the scan are still present and lead to higher melting enthalpies. It must be remembered that any cold crystallization of PLLA occurs at temperatures that overlap with the melting range of the PE block, as already explained above. A similar behavior has also been reported for PPDX-*b*-PCL block copolymers,[43,64] where coincident crystallization of both blocks could only be separated by self-nucleation of the PPDX block.

Close examination of Figure 1c shows that at the beginning of domain II (T_s = 176 °C) a slight decrease in the size of the cold crystallization exotherm (overlapped with the PE block melting endotherm) is obtained. At lower T_s temperatures this cold crystallization exotherm completely disappears because the PLLA chains already crystallized during cooling from the T_s (see Figure 1a). A similar melting behavior was found after slow cooling from the melt at 2 °C/min for the $L_{46}E_{54}^{50}$ block copolymer, where PLLA and PE block crystallizations could be separated; for details see ref 53.

The location of domain III was estimated by observing the subsequent heating scans after self-nucleation presented in Figure 1c. At 173 °C a slight broadening of the melting endotherm corresponding to the PLLA block is observed, indicating that a small population of crystals was annealed and are melting at higher temperatures. Therefore, the PLLA block at 173 °C is in domain III. Also, the fact that the crystallization started (Figure 1b) immediately after cooling from 173 °C is another classical sign of domain III. The annealed population grows upon decreasing T_s, and at 165 °C almost the entire population of PLLA crystals has been annealed as indicated by the sharp melting peak and lack of cold crystallization just before melting (note that in the melting curves for T_s temperatures higher than 165 °C, a very small cold crystallization exotherm appears just before the start of PLLA melting).

The locations of the three self-nucleation domains on top of a representative heating scan for the PLLA block within the $L_{46}E_{54}^{50}$ diblock copolymer and for PLLA homopolymer are shown in Figure 2. Müller et al.[2,65,66] have previously shown that domain II disappears for block copolymer systems where

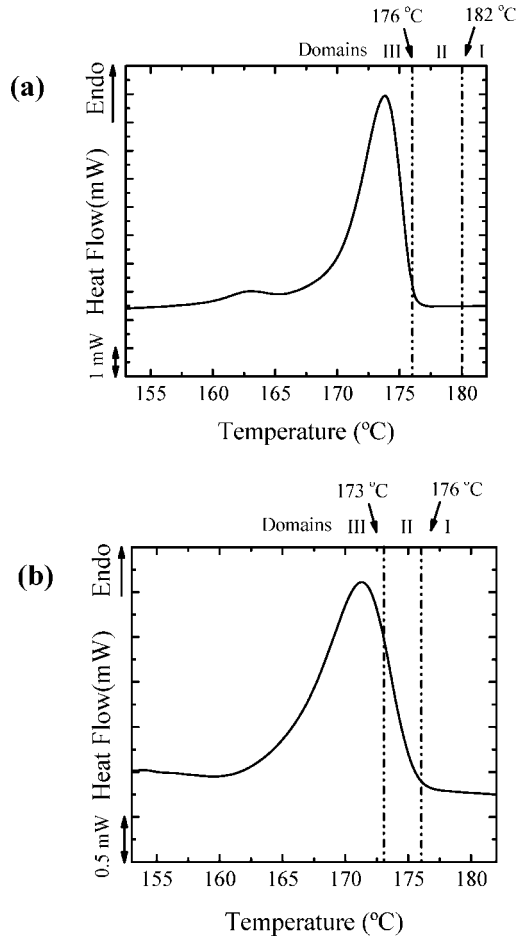

Figure 2. Self-nucleation domains for (a) PLLA and (b) the PLLA block within $L_{46}E_{54}^{50}$.

the crystallizable block (PE, PCL, or PEO) is strongly confined into small isolated microdomains; this is a direct result of the extremely high density of microdomains that need to be self-nucleated when the crystallizable block is confined within small isolated microdomains. The presence of domain II in the PLLA block indicate that homogeneous nucleation is not taking place for the PLLA block in spite of the confinement effect, in agreement with a lamellar morphology that contains defects that lead to percolated microdomains.[2] However, the temperatures for the transition between domains are decreased in the block copolymer as compared to homo-PLLA, pointing out that the processes of self-nucleation and annealing are more difficult due to the confinement effect.

Another interesting result is the effect of PLLA crystals on the PE block crystallization. Figure 3 shows the crystallization exotherms of the PE block after the self-nucleation of the PLLA block at the indicated T_s. At the beginning of domain II, where PLLA starts to crystallize in a separated exotherm, the crystallization temperature of the PE block also starts to shift to higher values (from 89.0 to 89.8 °C), and at lower T_s values, the crystallization temperature of the PE block increased to 90.5 °C. Polyethylene has an intrinsically high nucleation density that is difficult to increase; therefore, a shift of one or even half a degree in crystallization temperature can be a sign of a moderate nucleating effect. Thanks to the self-nucleation experiments, PLLA crystallization can now be separated from the coincident PLLA−PE crystallization during the cooling scan and the nucleating effect of PLLA crystals on the PE block is more clearly revealed. These results confirm previous reports found during slow cooling from the melt,[53] where separated crystallization of each component could be seen, and PE

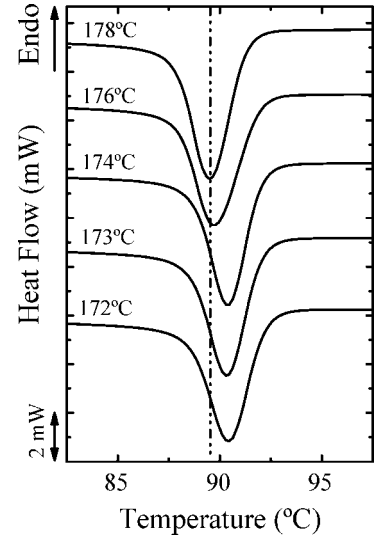

Figure 3. A close-up of Figure 1a around the crystallization temperature range of the PE block after self-nucleation of the PLLA block in $L_{46}E_{54}^{50}$.

nucleation within $L_{46}E_{54}^{50}$ was observed as compared to the PE block crystallization within $LD_{54}E_{46}^{60}$ block copolymer (in this last case no nucleation effect was seen as expected since PLDA is amorphous).

Isothermal Crystallization Kinetics. The overall isothermal crystallization kinetics of the crystalline components within the block copolymers, homo-PLLA and homo-PE were determined by DSC experiments. The results of fitting the DSC isothermal crystallization data by Avrami equation and the inverse of the half-crystallization times for both block copolymers and homopolymers were previously reported.[53,54] According to these results, a higher supercooling is needed to crystallize the PLLA block within PLLA-*b*-PE than homo-PLLA. The values of $1/\tau_{50\%}$ also indicate that the PLLA block crystallizes at much slower rates than homo-PLLA when similar crystallization temperatures are considered by extrapolation. Such a decrease in the overall crystallization rate of the PLLA block within the copolymer must be responsible for the coincident crystallization effect that can be observed when the PLLA-*b*-PE diblock copolymer is cooled down from the melt at rates larger than 2 °C/min.

For the PE block within the block copolymers and for homo-PE the crystallization rate of the PE block was reduced by amorphous PLDA or by semicrystalline PLLA.[53,54] However, in the case of PLLA-*b*-PE, the PLLA block was crystallized to saturation first; therefore, a nucleation effect of the PLLA crystals on the PE block must be present, as demonstrated above. Therefore, even though the crystallization kinetics of the PE block is depressed in the PLLA-*b*-PE diblock copolymer, the nucleation effect compensates this reduction, and in the end the PE block attached to the semicrystalline PLLA can crystallize faster than that attached to amorphous PLDA, even though one could anticipate a degree of confinement similar or higher (because of the presence of a crystalline phase) in the case of PLLA-*b*-PE as compared to PLDA-*b*-PE. In the case of another double-crystalline diblock copolymer system, i.e., PPDX-*b*-PCL, it was also found that the effect of the molten PCL chains depressed the crystallization rate of PPDX block with respect to homo-PPDX, and a nucleation effect of the crystallized PPDX on PCL block was also reported.[43]

We have tried to obtain the equilibrium melting temperature for PLLA and for the PLLA block within the PLLA-*b*-PE diblock copolymers, and we encounter difficulties related to the usual tendency of PLLA to reorganize during the scan. The

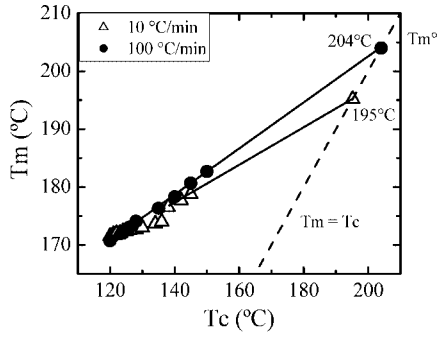

Figure 4. Hoffman−Weeks plot for homo-PLLA. The data were collected after isothermal crystallization by immediate heating from the crystallization temperature up to 190 °C at the indicated heating rates.

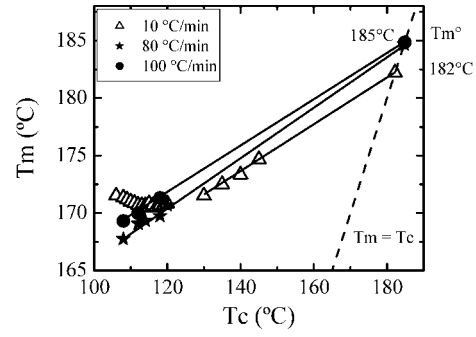

Figure 5. Hoffman−Weeks plot for the PLLA block within $L_{46}E_{54}^{50}$. The data were collected after isothermal crystallization by immediate heating from the crystallization temperature up to 190 °C at the indicated heating rates.

equilibrium melting temperature refers to the melting temperature of lamellar crystals with infinite thickness (or boundless crystals). Experimentally, it is very difficult to obtain lamellar crystals with infinite thickness. Therefore, the equilibrium melting temperature is generally obtained by extrapolation procedures.[67] The Hoffman and Weeks method is one of these procedures and involves linear extrapolation of experimental melting temperatures observed for various isothermal crystallization temperatures toward the equilibrium line $T_m = T_c$. Even though, strictly speaking, the Hoffman−Weeks extrapolation is only suitable for homopolymers because it does not consider the entropic contributions of chain conformations, this method has been frequently used to determine the equilibrium melting temperature in block copolymers due to its experimental and analytical simplicity. For example, Bogdanov et al.[68] used this extrapolation procedure to calculate the $T_m°$ of both blocks within PCL-*b*-PEO diblock copolymers; also Huang et al.[69] and Hong et al.[70] employed this technique with PLLA-*b*-PEO and PB-*b*-PEO diblock copolymers, respectively.

Figure 4 shows results for homo-PLLA employing a heating rate of 10 °C/min (the samples were first isothermally crystallized and then immediately reheated in the DSC to record their melting; see Experimental Section). The isothermal crystallization range was 120−150 °C. The data experiences a slope change at around 140 °C, and a lower slope was found at lower temperatures. Such behavior has already been reported in the literature for PLLA in similar crystallization ranges[71,72] and has been attributed to partial melting and reorganization during the scan. At higher crystallization temperatures, these effects are minimized by the long crystallization times and higher thermodynamic stability of the crystals generated. Therefore, we employed the data above 140 °C to perform the extrapolation in Figure 4 (data collected at 10 °C/min), and a value of 195 °C was obtained for $T_m°$; this value is similar to others previously reported in the literature.[71−74] As already mentioned in the Experimental Section, Pijpers et al.[57] proposed a high-speed DSC technique which is based on rate and mass compensation principles. Employing this method, we performed heating measurements on PLLA after isothermal crystallization at 100 °C/min in order to reduce reorganization processes during the scan. It is interesting to note in Figure 4 that the high-speed DSC data do not show a slope change, and if all the data points are employed for the extrapolation, we obtained a value for the equilibrium melting temperature of 204 °C, which could be closer to the real $T_m°$, since reorganization effects have been minimized.

Figure 5 presents similar results as those presented in Figure 4, but for the PLLA block within the $L_{46}E_{54}^{50}$ copolymer. The crystallization temperature range is reduced because of confinement effects. In this case, reorganization effects at lower T_c are even stronger, and for a temperature range in between 105 and 120 °C the data collected at 10 °C/min show almost no variation in apparent T_m values (even a small reduction in apparent melting points was detected in this temperature range). Confined crystallizable blocks have more difficulty in crystallizing and frequently undergo reorganization effects during the scan that are generally more pronounced than for parent homopolymers. Once more, if we increase the crystallization temperatures, we are able to find a temperature range where the apparent melting point increases as expected with crystallization temperature (see Figure 5; data collected at 10 °C/min in the temperature range above 125 °C). Using these data, an equilibrium melting point of 182 °C was obtained. This value is as expected lower than that found for homo-PLLA in view of the confinement effect.

If high-speed DSC is employed to avoid reorganization data, the equilibrium melting point can be found employing lower isothermal crystallization temperatures (which are more convenient since crystallization times are shorter), and the same value was obtained by extrapolating data collected at 80 and at 100 °C/min, i.e., 185 °C.

Morphology. The morphology was studied by SAXS and TEM for the $LD_{54}E_{46}^{60}$ and $L_{46}E_{54}^{50}$ diblock copolymers. For the $LD_{54}E_{46}^{60}$ two different crystallization temperatures were employed: 50 °C, which is below the glass transition temperature of the PLDA block; and 97 °C, a temperature 42 °C higher than $T_{g,PLDA}$ and where PE isothermal crystallization is also slow ($\tau_{50\%} \sim 8$ min).

Figure 6 shows the time-resolved Lorentz-corrected SAXS profiles of $LD_{54}E_{46}^{60}$ subjected to the crystallization process at 97 °C (a temperature above the T_g of PLDA and therefore a temperature for which a soft confinement environment is provided for the crystallization of the PE block). At 140 °C ($T_{m,PE}$) the SAXS profile displays mainly three diffraction peaks with the position ratio of 1:3:5, indicating that $LD_{54}E_{46}^{60}$ forms a lamellar morphology with the interlamellar distance (d) of 87 nm in the melt. The intensities of the even-order peak ($n = 2$, 4, 6) are weak because the volume fractions of the constituting blocks are ~0.5.[75] Using the density values of PLDA and PE ($\rho_{PLDA} = 1.154$ g/cm^3, $\rho_{PE} = 0.887$ g/cm^3),[76,77] the volume fraction of PLDA in $LD_{54}E_{46}^{60}$ is found to be 0.47, which is indeed close to 0.5. Similar results were obtained at 50 °C (results not shown), i.e., under hard confinement conditions for the PE block.

After quenching to the crystallization temperature, the PE blocks start to crystallize as evidenced by WAXS (results not shown). The corresponding SAXS profiles (Figure 6a) reveal that the lamellar morphology established in the melt remains essentially unperturbed upon PE crystallization for both crystallization temperatures, except that the scattering intensity drops slightly (Figure 6b). The decrease of intensity can be attributed

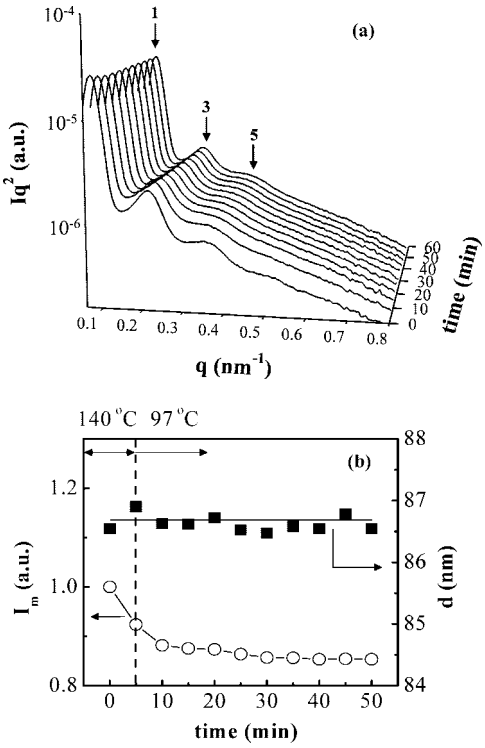

Figure 6. (a) Time-resolved Lorentz-corrected SAXS profiles. (b) Variations of the SAXS primary peak intensity (I_m) and the interlamellar distance (d) of $LD_{54}E_{46}^{60}$ during crystallization at 97 °C.

to the crystallization of PE blocks that reduces the electron density contrast between PE and PLDA lamellae.[78] The intensity decrease is however small because of the low degree of crystallinity (~10%) developed by the hydrogenated PE block at this high crystallization temperature. The SAXS/WAXS results hence reveal that the crystallization of the PE block was confined within the lamellar domains established by microphase separation in the melt. In summary, we can observe that crystallization in the different thermal histories employed cannot change the original lamellar structure present in the melt state because PLDA-*b*-PE is strongly segregated in the melt. Therefore, regardless of the confinement offered by the second block (hard or soft depending on crystallization conditions), the PE crystallites are confined within the preexisting lamellar domains established by microphase separation in the melt. Another possibility to the unaltered melt morphology would be the low crystallinity of the hydrogenated PE block during crystallization; however, no morphological breakout was detected for the PLLA-*b*-PE during PLLA crystallization in spite of its relatively high crystallinity (~50%), as will be shown later.

TEM images of $LD_{54}E_{46}^{60}$ annealed at 190 °C for 1 h and then quenched to −20 °C are shown in Figure 7 and confirm the SAXS data. Figure 7 shows a well-defined periodic lamellar structure for $LD_{54}E_{46}^{60}$. The sample was stained by RuO_4, which only stained the amorphous PLDA but not the PE crystals. Under the staining conditions employed, both amorphous and crystalline PE chains cannot be distinguished from each other. Therefore, the gray layers in the TEM image represent the PLDA microdomains and the bright ones represent the PE layers. One can see that the long period of the lamellar structure has a thickness around 61 ± 9 nm obtained by TEM, which is lower than that obtained by SAXS (87 nm). However, note that absolute lamellar thickness determined from TEM image could be inaccurate, since the viewing angle may not be orthogonal to the lamellar normal. In addition, interconnected lamellae of the same block were observed in TEM images, which can be considered as morphological defects that allow percolation and

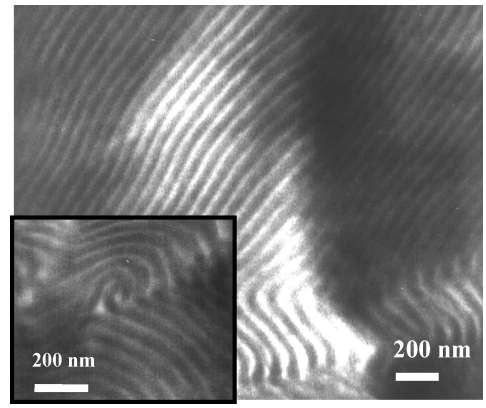

Figure 7. TEM micrograph of the $LD_{54}E_{46}^{60}$ diblock copolymer: gray, amorphous PLDA; light, semicrystalline PE.

dominant heterogeneous nucleation; this was confirmed by the sigmoidal crystallization kinetics obtained by DSC (results not shown).

We now turn our attention to the double-crystalline diblock copolymer case. Here we have examined the crystallization process under two types of cooling histories from the melt. The first type is called "two-stage crystallization", where the system was cooled from 190 °C (which is higher than $T_{m,PE}$ and $T_{m,PLLA}$) to 130 °C (which is higher than $T_{m,PE}$ but lower than $T_{m,PLLA}$) to allow PLLA crystallization followed by cooling to 97 °C to induce PE crystallization. The other type is called "one-stage crystallization", where the system was quenched directly from 190 to 80 °C, at which PLLA and PE blocks compete to crystallize.

Figure 8 shows the time-resolved SAXS and WAXS profiles of $L_{46}E_{54}^{50}$ subjected to the two-stage crystallization process. At 190 °C, the SAXS profile shows multiple peaks with position ratio of 1:2:3, indicating that $L_{46}E_{54}^{50}$ forms a lamellar morphology with the interlamellar distance of 72.2 nm in the melt. Since the volume fraction of PLLA in $L_{46}E_{54}^{50}$ is ca. 0.4, the second-order peak is visible in the SAXS pattern. Upon cooling to 130 °C, the crystallinity of PLLA block is not detectable until 15 min have elapsed, as indicated by the WAXS profiles and the temporal development of the relative crystallinity in Figure 8c,d. The PE blocks remain essentially molten over the holding time (i.e., 35 min) at this temperature.

The SAXS peaks shift to lower q immediately after the system reached 130 °C. This position shift corresponds to an increase of d by 6.3 nm or a reduction of the cross-sectional area per junction point from 0.58 to 0.51 nm^2. Since the swelling of the interlamellar distance takes place before the development of PLLA crystallinity, it should not arise from the crystallization of PLLA; alternatively, the increase of d is attributed to the increasing stretching of both amorphous PLLA and PE blocks normal to the lamellar interface due to the increase of χ on lowering the temperature.[79]

As can be seen from Figure 8e, the interlamellar distance remains approximately at 78.5 nm during the course of PLLA crystallization, indicating that the crystallization of PLLA is effectively confined within the lamellar microdomains although the surrounding PE domains are rubbery at 130 °C. This confinement effect is again due to the large segregation strength between PLLA and PE. It is noted that, in contrast to the $LD_{54}E_{46}^{60}$ system, the intensity of the primary scattering peak is virtually unaffected by the PLLA crystallization, because the enhancement of electron density contrast due to the development of PLLA crystallites is small considering that crystalline and amorphous PLLA have very similar electron densities.[78,80]

The crystallization of PE blocks occurs rapidly when the system is subsequently cooled to 97 °C. During the PE

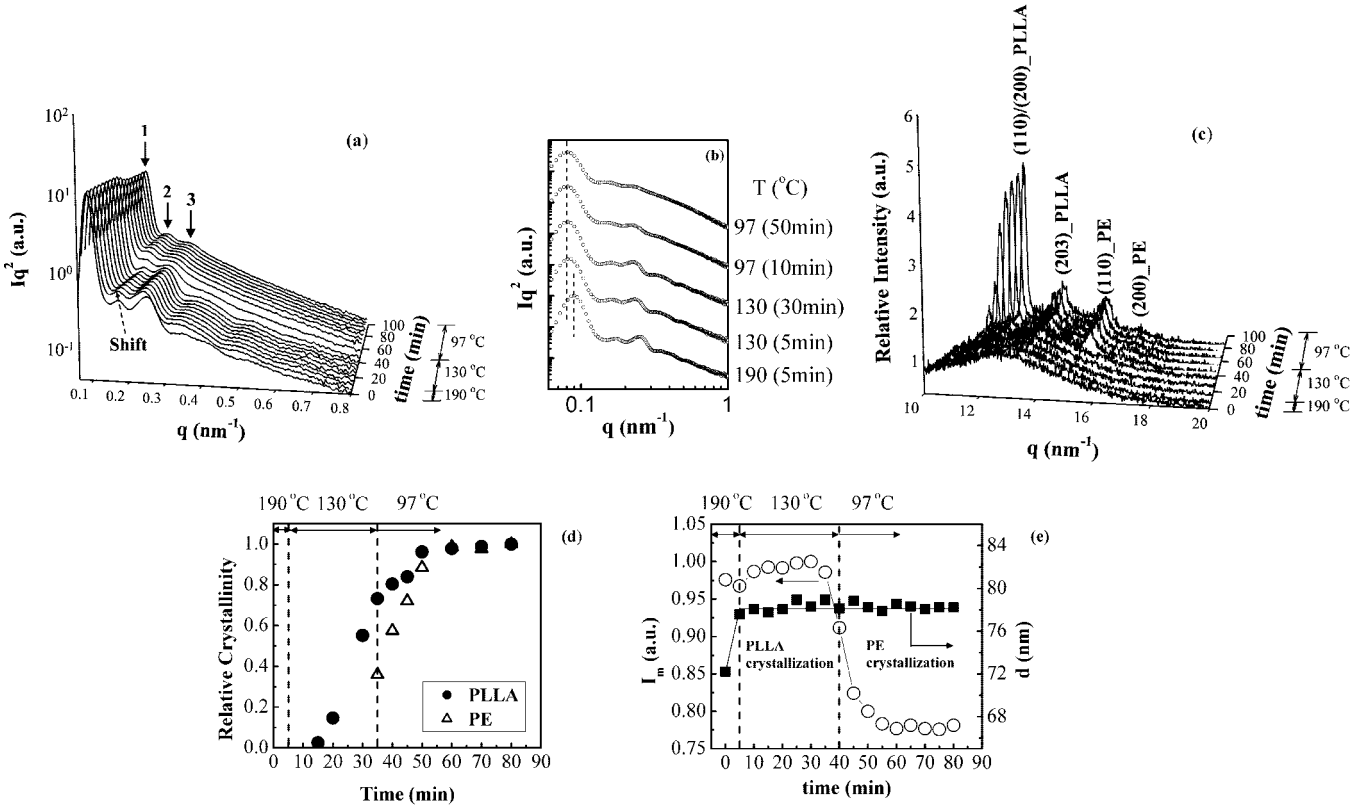

Figure 8. (a) Time-resolved Lorentz-corrected SAXS profiles. (b) 1-D Lorentz-corrected SAXS profiles of $L_{46}E_{54}^{50}$ cooled from 190 to 130 °C. The SAXS peaks shift to lower q immediately after the system reached 130 °C. This position shift corresponds to an increase of d by 6.3 nm. (c) Time-resolved WAXS profiles. (d) The developments of the crystallinities of PLLA and PE blocks during the crystallization. (e) Variations of the SAXS primary peak intensity (I_m) and the interlamellar distance (d) of $L_{46}E_{54}^{50}$ subjecting to a two-stage crystallization. The system was cooled from 190 to 130 °C to allow PLLA crystallization for 35 min followed by cooling to 97 °C to induce PE crystallization.

crystallization, the SAXS peaks broaden but their positions remain unperturbed. This indicates that PE crystallites develop within the confined space established by the prior crystallization of the PLLA component. The crystallization of PE blocks merely distorts the order of lamellar stacking slightly. Figure 8e demonstrates that the SAXS intensity drops abruptly as soon as the crystallization of PE blocks occurs. The reduction in the SAXS intensity is again originated from the decreasing electron density contrast between the crystalline phases of PLLA and PE during the second cooling stage (130 to 97 °C).

Finally, we also reheated the sample to melt the two blocks and to ensure that the morphology was able to come back to that originally exhibited by the melt state (results not shown). This is the expected behavior of a block copolymer that is strongly segregated from its corresponding covalently bonded neighbor and as in this case forms microphase-separated lamellae where the crystallization of each component has to occur in the confined space defined by the phase-separated microdomains.

Figure 9 shows the time-resolved SAXS/WAXS results of $L_{46}E_{54}^{50}$ subjecting to one-stage crystallization (direct quench from 190 to 80 °C). After quenching to 80 °C, both blocks are able to crystallize; however, the PE block crystallizes faster than the PLLA block in spite of the higher crystallization temperature of the PLLA block, as revealed by the WAXS profiles. Figure 9d plots the relative crystallinities of both blocks as a function of time at 80 °C. PE block is found to crystallize immediately upon reaching 80 °C, and its crystallinity reaches saturation after only 15 min. The immediate crystallization of PE block is accompanied by an abrupt drop of the intensity of the SAXS primary peak, as shown in Figure 9e. On the other hand, PLLA starts to crystallize at around 15 min and finishes its crystallization process after 40 min.

The primary SAXS peak is found to slightly shift to lower q upon crystallization of PE block, which corresponds to a small increase of d by 1.7 nm (see also Figure 9e). In principle, the even larger increase of χ on cooling to 80 °C should result in an increase of d larger than 6.3 nm observed for the previous case of cooling to 130 °C. We propose that in the present case the stretching of the block chains caused by increasing χ is outweighed by the very rapid crystallization of PE, such that the observed interlamellar distance is governed by the PE crystallite thickness coupled with the conformation of the temporarily uncrystalline PLLA bocks under the cross-sectional area of the junction point prescribed by the crystallite size. After 15 min, the PLLA block starts to crystallize within the remaining confined space determined by the leading crystallizing PE component, and the latterly crystallized PLLA block can no longer perturb the confined space as the evidenced by the invariance of the corresponding SAXS profiles.

In Figure 10 TEM micrograph for the $L_{46}E_{54}^{50}$ block copolymer cooled from the melt and crystallized in one step at 80 °C is shown. Small crystals roughly oriented can be observed corresponding to PE crystallites; dark zones correspond to PE amorphous chains and PLLA block. Because of crystallization conditions, the degree of crystallinity of PLLA block is expected to be low, and the small crystallites of PLLA could not be resolved by the staining conditions employed. In the case of the $LD_{54}E_{46}^{60}$ block copolymer, the TEM micrograph previously shown (Figure 7) was obtained after quenching to −20 °C from the melt; in this case the PE lamellae were too small and cannot be distinguished. In other words, the PE block within $L_{46}E_{54}^{50}$ was isothermally crystallized at 80 °C, and therefore the lamellar crystals within the microdomain structure could be observed by TEM, although with a disordered pattern due to the fast crystallization kinetics of PE chains.

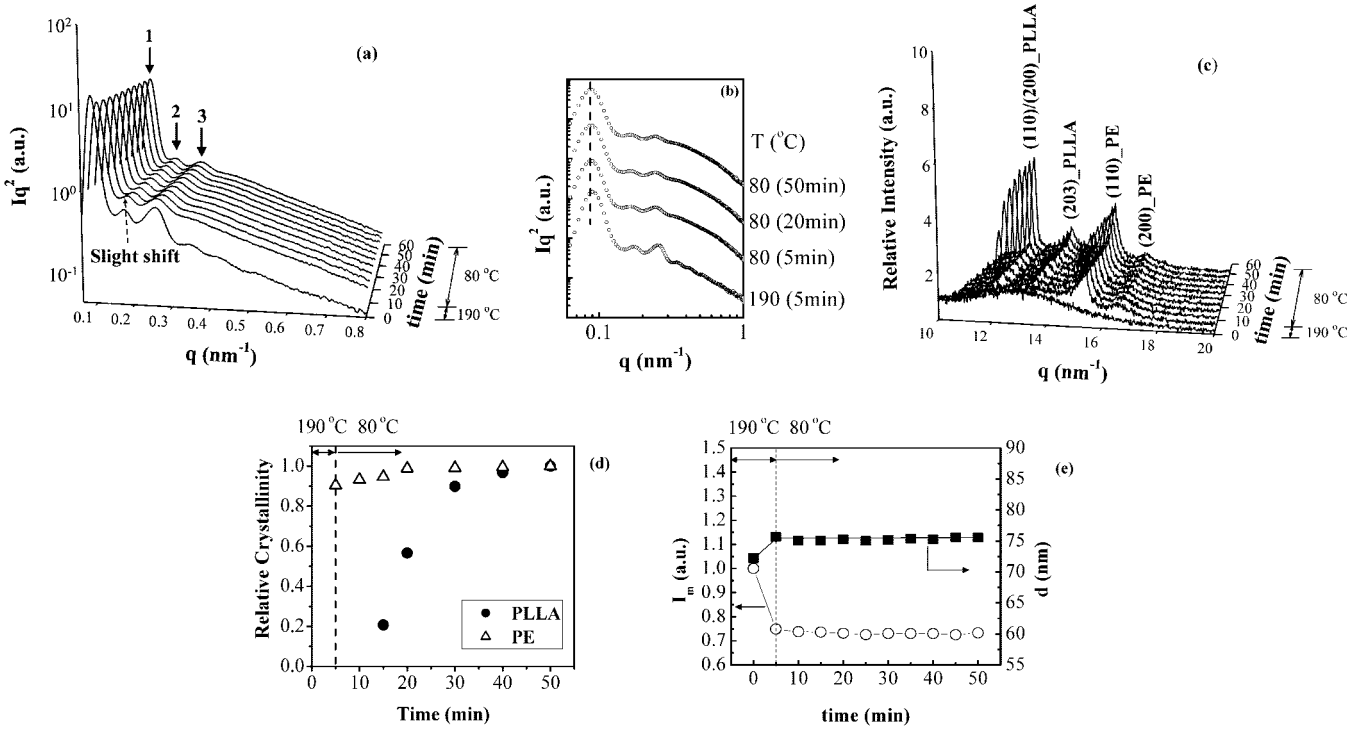

Figure 9. (a) Time-resolved Lorentz-corrected SAXS profiles. (b) 1-D Lorentz-corrected SAXS profiles of $L_{46}E_{54}^{50}$ cooled from 190 to 80 °C. The primary SAXS peak is found to slight shift to lower q upon crystallization of PE block, which corresponds to a small increase of d by 1.7 nm. (c) Time-resolved WAXS profiles. (d) The developments of the crystallinities of PLLA and PE blocks during the crystallization. (e) Variations of the SAXS primary peak intensity (I_m) and the interlamellar distance (d) of $L_{46}E_{54}^{50}$ subjecting to a one-stage crystallization. The system was cooled directly from 190 to 80 °C to allow the crystallizations of both PLLA and PE blocks.

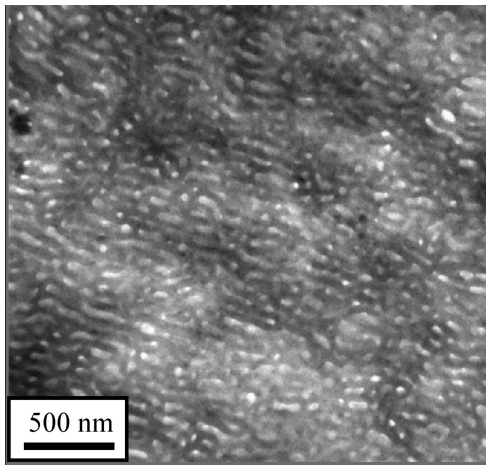

Figure 10. TEM micrograph of the $L_{46}E_{54}^{50}$ diblock copolymer cooled from the melt and crystallized in one step at 80 °C.

We have shown that in $LD_{54}E_{46}^{60}$ the overall melt structure was preserved during PE block crystallization independently of whether the noncrystallizing PLDA block was glassy or rubbery. A similar scenario is observed for the double-crystalline $L_{46}E_{54}^{50}$ irrespective of the crystallization histories studied here. In the case of two-step crystallization, the increase of χ upon the first-stage cooling from 190 to 130 °C resulted in a swelling of the lamellar microdomains by 6.3 nm before PLLA crystallization sets in. The crystallization of PLLA blocks then occurred and was effectively confined within this lamellar environment without introducing obvious perturbation of the microdomain structure and interlamellar distance, although the surrounding molten PE domains were soft. When the PE block crystallized later upon further cooling to 97 °C, the crystallization of PE block occurred within the remaining space without altering the confined space because the PLLA lamellar domains containing the crystallites displayed a hard confinement effect on PE blocks. When $L_{46}E_{54}^{50}$ was cooled directly from 190 to 80 °C, both blocks could crystallize, but the PLLA block must crystallize within the confined space formed in between the PE crystalline lamellae which were formed earlier and in consequence the melt morphology was almost unperturbed. When PE crystallized first, the crystallites containing PE domains produced a hard confinement for the PLLA block crystallization which occurred gradually, and therefore it was more difficult for the PLLA to distort the microdomain morphology.

Conclusions

Strongly segregated PLA-*b*-PE diblock copolymers form lamellar microdomains as evidenced by TEM and SAXS results. The crystalline blocks can crystallize within the confinement of their lamellar microdomains without forming spherulites in view of the strong segregation in between the blocks. The SAXS results revealed that the crystallization of the PE block was strictly confined within the preexisting lamellar microdomains established by microphase separation in the melt regardless of whether $T_{c,PE} > T_{g,PLDA}$ (soft confinement) or $T_{c,PE} < T_{g,PLDA}$ (hard confinement). In the case of PLLA-*b*-PE double-crystalline system, a coincident crystallization process was detected when they were cooled from the melt at rates exceeding 2 °C /min. This behavior was caused by the reduction in PLLA overall crystallization kinetics induced by the attached molten PE block. When the PLLA block was self-nucleated, the two crystallization processes of PLLA and PE blocks were separated, and the nucleating effect of the PLLA crystals on the PE block was demonstrated. Two kinds of cooling process were performed in time-resolved SAXS and WAXS measurement for this double-crystalline system. In two-stage crystallization of PLLA-*b*-PE, the PLLA blocks crystallized first without introducing obvious perturbation on the melt morphology; the crystallization of PE block followed later. Because the previously crystallized

PLLA offered a hard confinement effect that fixed the morphology, the crystallization of the PE block occurred without any further modification of the microdomain structure. In a one-stage crystallization of PLLA-*b*-PE, the PE block crystallized much faster than the PLLA block and fixed the morphology (hard confinement), so at the end of the crystallization period of the PLLA block the swelling of interlamellar distance was only 1.7 nm.

Acknowledgment. We thank Kelly Anderson for the synthesis of the block copolymers used in this study. We also thank Marc Rodwogin for his help with an initial morphology determination by SAXS. The USB team acknowledges financial support from Decanato de Investigación y Desarrollo of Simón Bolívar University through Grant DID-GID-02. The NTHU team acknowledges the support from the National Science Council under Grant NSC 96-2221-E-007-022.

References and Notes

(1) Hamley, I. W. *The Physics of Block Copolymers*; Oxford University Press: New York, 1998; Chapter 5.
(2) Müller, A. J.; Balsamo, V.; Arnal, M. L. *Adv. Polym. Sci.* **2005**, *190*, 1–63.
(3) Müller, A. J.; Balsamo, V.; Arnal, M. L. In *Lecture Notes in Physics: Progress in Understanding of Polymer Crystallization*; Reiter, G., Strobl, G., Eds.; Springer: Berlin, 2007; Springer Lecture Notes in Physics Vol. 714, pp 229−259.
(4) Ryan, A. J.; Fairclough, J. P. A.; Hamley, I. W.; Mai, S. M.; Booth, C. *Macromolecules* **1997**, *30*, 1723–1727.
(5) Ryan, A. J.; Hamley, I. W.; Bras, W.; Bates, F. S. *Macromolecules* **1995**, *28*, 3860–3868.
(6) Quiram, D. J.; Register, R. A.; Marchand, G. R. *Macromolecules* **1997**, *30*, 4551–4558.
(7) Quiram, D. J.; Register, R. A.; Marchand, G. R.; Ryan, A. J. *Macromolecules* **1997**, *30*, 8338–8343.
(8) Hamley, I. W.; Fairclough, J. P. A.; Terrill, N. J.; Ryan, A. J.; Lipic, P. M.; Bates, F. S.; Towns-Andrews, E. *Macromolecules* **1996**, *29*, 8835–8843.
(9) Nojima, S.; Kato, K.; Yamamoto, S.; Ashida, T. *Macromolecules* **1992**, *25*, 2237–2242.
(10) Sakurai, K.; MacKnight, W. J.; Lohse, D. J.; Schulz, N.; Sissano, J. A. *Macromolecules* **1994**, *27*, 4941–4951.
(11) Liu, L. Z.; Yeh, R.; Chu, B. *Macromolecules* **1996**, *29*, 5336–5345.
(12) Rangarajan, P.; Register, R. A.; Fetters, L. J.; Bras, W.; Naylor, S.; Ryan, A. J. *Macromolecules* **1995**, *28*, 4932–4938.
(13) Nojima, S.; Hashizume, K.; Rohadi, A.; Sasaki, S. *Polymer* **1997**, *38*, 2711–2718.
(14) Chen, H. L.; Wu, J. C.; Lin, J. S. *Macromolecules* **2001**, *34*, 6936–6944.
(15) Shiomi, T.; Tsukada, H.; Takeshita, H.; Takenaka, K.; Tezuka, Y. *Polymer* **2001**, *42*, 4997–5004.
(16) Shiomi, T.; Takeshita, H.; Kawaguchi, H.; Nagai, M.; Takenaka, K.; Miya, M. *Macromolecules* **2002**, *35*, 8056–8065.
(17) Huang, P.; Zhu, L.; Guo, Y.; Ge, Q.; Jing, A. J.; Chen, W. Y.; Quirk, R. P.; Cheng, S. Z. D.; Thomas, E. L.; Lotz, B.; Hsiao, B. S.; Avila-Orta, C. A.; Sics, I. *Macromolecules* **2004**, *37*, 3689–3698.
(18) Zhu, L.; Cheng, S. Z. D.; Calhoun, B. H.; Ge, Q.; Quirk, R. P.; Thomas, E. L.; Hsiao, B. S.; Yeh, F.; Lotz, B. *J. Am. Chem. Soc.* **2000**, *122*, 5957–5967.
(19) Takeshita, H.; Ishii, N.; Araki, C.; Miya, M.; Takenaka, K.; Shiomi, T. J. *J. Polym. Sci., Part B* **2004**, *42*, 4199–4206.
(20) Muthukumar, M.; Ober, C. K.; Thomas, E. L. *Science* **1997**, *277*, 1225–1232.
(21) Hamley, I. W. *Adv. Polym. Sci.* **1999**, *148*, 113–137.
(22) Ryan, A. J.; Hamley, I. W.; Bras, W.; Bates, F. S. *Macromolecules* **1995**, *28*, 3860–3868.
(23) Richardson, P. H.; Richards, R. W.; Blundell, D. J.; MacDonald, W. A.; Mills, P. *Polymer* **1995**, *36*, 3059–3069.
(24) Loo, Y. L.; Register, R. A.; Ryan, A. J. *Macromolecules* **2002**, *35*, 2365–2374, and references therein.
(25) Müller, A. J.; Balsamo, V.; Arnal, M. L.; Jakob, T.; Schmalz, H.; Abetz, V. *Macromolecules* **2002**, *35*, 3048–3058, and references therein.
(26) Nojima, S.; Toei, M.; Hara, S.; Tanimoto, S.; Sasaki, S. *Polymer* **2002**, *43*, 4087–4090.
(27) Reiter, G.; Castelein, G.; Sommer, J. U.; Rottele, A.; Thurn-Albrecht, T. *Phys. Rev. Lett.* **2001**, *87*, 226101.
(28) Arnal, M. L.; Balsamo, V.; Lopez-Carrasquero, F.; Contreras, J.; Carrillo, M.; Schmalz, H.; Abetz, V.; Laredo, E.; Müller, A. J. *Macromolecules* **2001**, *34*, 7973–7982.
(29) Zhu, L.; Cheng, S. Z. D.; Calhoun, B. H.; Ge, Q.; Quirk, R. P.; Thomas, E. L.; Hsiao, B. S.; Yeh, F.; Lotz, B. *Polymer* **2001**, *42*, 9121–9131.
(30) Weimann, P. A.; Hajduk, P. A.; Hajduk, D. A.; Chu, C.; Chaffin, K. A.; Brodil, J. C.; Bates, F. S. *J. Polym. Sci., Part B: Polym. Phys.* **1999**, *37*, 2053–2068.
(31) Chen, H. L.; Hsiao, S. C.; Lin, T. L.; Yamauchi, K.; Hasegawa, H.; Hashimoto, T. *Macromolecules* **2001**, *34*, 671–674.
(32) Zhou, S.; Deng, X.; Yang, H. *Biomaterials* **2003**, *24*, 3563–3570.
(33) Bae, S. J.; Suh, J. M.; Sohn, Y. S.; Bae, Y. H.; Kim, S. W.; Jeong, B. *Macromolecules* **2005**, *38*, 5260–5265.
(34) Sun, J.; Chen, X.; He, C.; Jing, X. *Macromolecules* **2006**, *39*, 3717–3719.
(35) Zhu, W.; Xie, W.; Tong, X.; Shen, Z. *Eur. Polym. J.* **2007**, *43*, 3522–3530.
(36) Li, L.; Meng, F.; Zhong, Z.; Byelov, D.; de Jeu, W. H.; Feijen, J. *J. Chem. Phys.* **2007**, *126*, 024904.
(37) Li, S. M.; Rashkov, I.; Espartero, J. L.; Manolova, N.; Vert, M. *Macromolecules* **1996**, *29*, 57–62.
(38) Sun, J.; Hong, Z.; Yang, L.; Tang, Z.; Chen, X.; Jing, X. *Polymer* **2004**, *45*, 5969–5977.
(39) Shin, D.; Shin, K.; Aamer, K. A.; Tew, G. N.; Russell, T. P.; Lee, J. H.; Jho, J. Y. *Macromolecules* **2005**, *38*, 104–109.
(40) Kim, J. K.; Park, D.-J.; Lee, M.-S.; Ihn, K. J. *Polymer* **2001**, *42*, 7429–7441.
(41) Wang, J.-L.; Dong, C.-M. *Macromol. Chem. Phys.* **2006**, *207*, 554–562.
(42) Albuerne, J.; Márquez, L.; Müller, A. J.; Raquez, J.-M.; Degée, Ph.; Dubois, Ph.; Castelletto, V.; Hamley, I. *Macromolecules* **2003**, *36*, 1633–1644.
(43) Müller, A. J.; Albuerne, J.; Márquez, L.; Raquez, J.-M.; Degée, Ph.; Dubois, Ph.; Hobbs, J.; Hamley, I. W. *Faraday Discuss.* **2005**, *128*, 231–252.
(44) Hamley, W.; Castelletto, V.; Castillo, R. V.; Müller, A. J.; Martin, C. M.; Pollet, E.; Dubois, Ph. *Macromolecules* **2005**, *38*, 463–472.
(45) Hamley, I. W.; Parras, P.; Castelletto, V.; Castillo, R. V.; Müller, A. J.; Pollet, E.; Dubois, Ph.; Martin, C. M. *Macromol. Chem. Phys.* **2006**, *207*, 941–953.
(46) Castillo, R. V.; Arnal, M. L.; Muller, A. J.; Hamley, I. W.; Castelletto, V.; Schmalz, H.; Abetz, V. *Macromolecules* **2008**, *41*, 879–889.
(47) Nojima, S.; Akutsu, Y.; Akaba, M.; Tanimoto, S. *Polymer* **2005**, *46*, 4060–4067.
(48) Sun, L.; Liu, Y.; Zhu, L.; Hsiao, B. S.; Avila-Orta, C. A. *Polymer* **2004**, *45*, 8181–8193.
(49) Hillmyer, M. A.; Bates, F. S. *Macromol. Symp.* **1997**, *117*, 121–130.
(50) Takeshita, H.; Fukumoto, K.; Ohnishi, T.; Ohkubo, T.; Miya, M.; Takenaka, K.; Shiomi, T. *Polymer* **2006**, *47*, 8210–8218.
(51) Ring, J. O.; Thomann, R.; Mülhaupt, R.; Raquez, J.-M.; Degée, Ph.; Dubois, Ph. *Macromol. Chem. Phys.* **2007**, *208*, 896–902.
(52) Lim, J. Y.; Hansen, J. C.; Siedlecki, C. A.; Hengstebeck, R. W.; Cheng, J.; Winograd, N.; Donahue, H. J. *Biomacromolecules* **2005**, *6*, 3319–3327.
(53) Müller, A. J.; Castillo, R. V.; Hillmyer, M. *Macromol. Symp.* **2006**, *242*, 174–181.
(54) Müller, A. J.; Lorenzo, A. T.; Castillo, R. V.; Arnal, M. L.; Boschetti-de-Fierro, A.; Abetz, V. *Macromol. Symp.* **2006**, *245*, 154–160.
(55) Wang, Y.; Hillmyer, M. A. *J. Polym. Sci., Part A: Polym. Chem.* **2001**, *39*, 2755–2766.
(56) Anderson, K. S.; Hillmyer, M. A. *Polymer* **2004**, *45*, 8809–8823.
(57) Pijpers, T. F. J.; Mathot, V. B. F.; Goderis, B.; Scherrenberg, R. L.; van der Vegte, E. W. *Macromolecules* **2002**, *35*, 3601–3613.
(58) Ueda, M.; Sakurai, K.; Okamoto, S.; Lohse, D.; MacKnight, W. J.; Shinkai, S.; Sakurai, S.; Nomura, S. *Polymer* **2003**, *44*, 6995–7005.
(59) Mano, J. F.; Góme, Z.; Ribelles, J. L.; Alves, N. M.; Salmeró, N.; Sanchez, M. *Polymer* **2005**, *46*, 8258–8265.
(60) Kanchanasopa, M.; Runt, J. *Macromolecules* **2004**, *37*, 863–871.
(61) Fillon, B.; Wittman, J. C.; Lotz, B.; Thierry, A. *J. Polym. Sci., Part B* **1993**, *31*, 1383–1393.
(62) Müller, A. J.; Balsamo, V.; Arnal, M. L.; Jakob, T.; Schmalz, H.; Abetz, V. *Macromolecules* **2002**, *35*, 3048–3058.
(63) Lorenzo, A. T.; Arnal, M. L.; Sánchez, J. J.; Müller, A. J. *J. Polym. Sci., Part B: Polym. Phys.* **2006**, *44*, 1738–1750.
(64) Müller, A. J.; Albuerne, J.; Esteves, L. M.; Márquez, L.; Raquez, J.-M.; Degée, Ph.; Dubois, Ph.; Collings, S.; Hamley, I. W. *Macromol. Symp.* **2004**, *215*, 369–382.
(65) Balsamo, V.; Paolini, Y.; Ronca, G.; Müller, A. J. *Macromol. Chem. Phys.* **2000**, *201*, 2711–2720.
(66) Schmalz, H.; Müller, A. J.; Abetz, V. *Macromol. Chem. Phys.* **2003**, *204*, 111–124.
(67) Shultz, J. M. *Polymer Crystallization*; Oxford University Press: Oxford, 2001; pp 35−36.

(68) Bogdanov, B.; Vidts, A.; Schacht, E.; Berghmans, H. *Macromolecules* **1999**, *32*, 726–731.
(69) Huang, C.-I.; Tsai, S.-H.; Chen, C.-M. *J. Polym. Sci., Part B: Polym. Phys.* **2006**, *44*, 2438–2448.
(70) Hong, S.; Yang, L.; MacKnight, W. J.; Gido, S. P. *Macromolecules* **2001**, *34*, 7009–7016.
(71) Kalb, B.; Pennings, A. J. *Polymer* **1980**, *21*, 607–612.
(72) Iannace, S.; Nicolais, L. *J. Appl. Polym. Sci.* **1997**, *64*, 911–919.
(73) Tsuji, H.; Ikada, Y. *Polymer* **1995**, *36*, 2709–2716.
(74) Vasanthakumari, R.; Pennings, A. J. *Polymer* **1983**, *24*, 175–178.
(75) Roe, R. J. *Methods of X-ray and Neutron Scattering in Polymer Science*; Oxford University Press: New York, 2000; Vol. 196.
(76) Witzke, D. R.; Narayan, R.; Kolstad, J. J. *Macromolecules* **1997**, *30*, 7075–7085.
(77) Grulke, E. A. In *Polymer Handbook*, 4th ed.; Brandrup, J., Immergut, E. H., Grulke,E. A., Eds.; J. Wiley & Sons: New York, 1999; p VII/675.
(78) The electron densities of crystalline and amorphous PE are 0.576 and 0.507 mol e/cm^3, respectively, and those of crystalline PLLA and amorphous PLLA (or PLDA) are 0.676 and 0.661 mol e/cm^3, respectively. Therefore, the electron density contrast between PLDA and amorphous PE domains is 0.154 mol e/cm^3, while that between PLDA and crystalline PE domains (assuming 100% crystallinity) is 0.085 mol e/cm^3.
(79) Tanaka, H.; Hashimoto, T. *Macromolecules* **1991**, *24*, 5713.
(80) Chen, H. L.; Liu, H. H.; Lin, J. S. *Macromolecules* **2000**, *33*, 4856.

MA800859Y